Stability and Robustness Analysis of Plug-Pulling using an Aerial Manipulator

Jeonghyun Byun[1], Dongjae Lee[1], Hoseong Seo[1], Inkyu Jang[1], Jeongjun Choi[1] and H. Jin Kim[1]

***Abstract*— In this paper, an autonomous aerial manipulation task of pulling a plug out of an electric socket is conducted, where maintaining the stability and robustness is challenging due to sudden disappearance of a large interaction force. The abrupt change in the dynamical model before and after the separation of the plug can cause destabilization or mission failure. To accomplish aerial plug-pulling, we employ the concept of hybrid automata to divide the task into three operative modes, i.e, wire-pulling, stabilizing, and free-flight. Also, a strategy for trajectory generation and a design of disturbance-observer-based controllers for each operative mode are presented. Furthermore, the theory of hybrid automata is used to prove the stability and robustness during the mode transition. We validate the proposed trajectory generation and control method by an actual wire-pulling experiment with a multirotor-based aerial manipulator.**

I. INTRODUCTION

Aerial manipulation has been a growing research topic which aims to utilize the maneuverability of an aerial vehicle and the versatility of a robotic manipulator. Different from physically non-interacting passive tasks such as surveillance and remote sensing, an aerial manipulator can execute active tasks involving physical interaction such as grasping [1], [2], valve turning [3], drawer opening [4], contact inspection [5], transportation [6], [7], and door opening [8].

Despite various demonstrations of aerial manipulation tasks involving contact with environments, they usually involved a relatively low level of changes in the dynamic characteristics, and they rarely dealt with the transition during the physical interaction explicitly. In fact, there is a lack of research on the stability of aerial manipulation before and after the physical interaction. When a mode switch entails a significant change in the system response, neglecting it can lead to destabilization. Therefore, it is necessary to systematically analyze dynamical modes and design a robust controller to more realistically embrace the whole operation.

As an example of aerial manipulation involving a drastic change in dynamics, this paper deals with the problem of pulling a plug from a socket using a multirotor equipped with a two degree-of-freedom (DOF) robotic arm. In this task, the large force exerted on the end-effector suddenly disappears after the plug is separated from the socket. For formal analysis of the stability, we first formulate hybrid automata [9] which enclose all the dynamic models and the operative modes that have their own control laws different from another. Then, we design disturbance-observer (DOB)-based controllers [10] for the respective operative modes and prove the stability and robustness of the formulated hybrid automata [11].

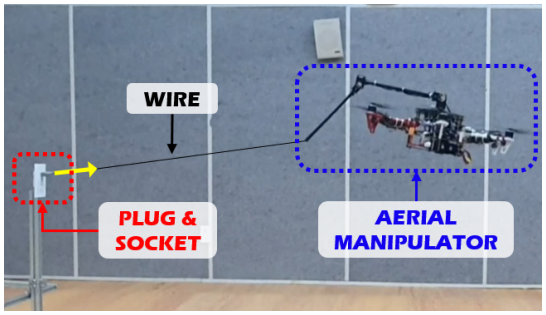

Fig. 1: An aerial manipulator, a multirotor equipped with a 2-DOF robotic arm, is pulling a plug from a socket. The plug is connected to a wire grabbed by the end effector of the aerial manipulator.

A. Related Works

There have been several works which explain aerial vehicles using the concept of hybrid automata. In [12], [13], [14], the contact task using an aerial vehicle is divided into two operative modes, i.e. docking and free-flight, and each mode are controlled by a different controller from one another. However, these works did not conduct an analysis on stability and robustness and the transition between those modes was not explicitly discussed.

Some studies addressed the stability and robustness of an aerial vehicle involved in the physical interaction using the hybrid automata theory. In [15], the stability of path-following control considering mode changes was investigated for a robust contact of a ducted-fan aerial vehicle on a vertical surface. In [16], the process of a multirotor landing on the slope was divided into several modes and the stability and robustness was proved in a similar way to [15]. However, in such settings, the effect of dynamic change can be reduced by slowly approaching the wall or landing site. Thus, there is no guarantee that such control methods can maintain the stability and robustness of the aerial manipulation involving an abrupt change such as plug-pulling.

This research was supported by Unmanned Vehicles Core Technology Research and Development Program through the National Research Foundation of Korea(NRF) and Unmanned Vehicle Advanced Research Center(UVARC) funded by the Ministry of Science and ICT, the Republic of Korea(NRF-2020M3C1C1A01086411).

This material is based upon work supported by the Ministry of Trade, Industry & Energy(MOTIE, Korea) under Industrial Technology Innovation Program. No.10067206, 'Development of Disaster Response Robot System for Lifesaving and Supporting Fire Fighters at Complex Disaster Environment'.

[1] The authors are with the Department of Aerospace Engineering and Automation and System Research Institute (ASRI), Seoul National University, Seoul, South Korea. {quswjdgus97, ehdwo713, hosung37, leplusbon, lojol2327, hjinkim}@snu.ac.kr

B. Contributions

To the best of the authors' knowledge, this is the first attempt to conduct a plug-pulling task using an aerial manipulator, which involves a significant mode change, and present a thorough analysis on the stability and robustness of the aerial manipulator using the hybrid automata theory. We propose a trajectory generation strategy and DOB control structure for each operative mode. Especially, for the situation of pulling the wire, we derive a dynamical model of the aerial manipulator constrained to the wire and the socket. In addition, we construct a DOB structure corresponding to the model of the plug-pulling aerial manipulator and prove the stability and robustness of the proposed controller.

C. Outline

In Section II, we briefly explain the concept of hybrid automata, describe notions utilized throughout the paper and introduce the aerial plug-pulling scenario. Section III formulates hybrid automata for the aerial manipulator conducting the plug task, and the trajectory generation and controller design is described in Section IV. Section V shows the stability and robustness analysis, and Section VI presents the experimental setup and results.

II. PROBLEM SETUP

A. Preliminary: Hybrid Automata

The following elements define *hybrid automata* [9] with the state variable $x \in \mathbb{R}^{n_x}$ and the control input $u_x \in \mathbb{R}^{m_x}$.

- *Set of operative modes*, $\mathcal{M}$, contains names of the control modes. With respect to $\mathcal{M}$, we let $t_{0,\mu}$ and $t_{d,\mu}$ denote the time when the mode μ begins and the desired time to terminate the mode μ, respectively.
- *Domain mapping*, $\mathcal{D} : \mathcal{M} \rightrightarrows \mathbb{R}^{n_x} \times \mathbb{R}^{m_x}$, means the possible region where x and u_x can evolve while maintaining a specific mode μ. It is expressed as $\mathcal{D}(\mu) = \mathcal{D}_x(\mu) \times \mathcal{D}_{u_x}(\mu)$.
- *Flow map*, f: $\mathcal{M} \times \mathbb{R}^{n_x} \times \mathbb{R}^{m_x} \to \mathbb{R}^{n_x/2}$, describes the dynamics in each operative mode μ.
- *Set of edges*, $\mathcal{E} \subset \mathcal{M} \times \mathcal{M}$, means all possible pairs of operative mode changes (μ_1, μ_2).
- *Guard mapping*, $\mathcal{G} : \mathcal{E} \rightrightarrows \mathbb{R}^{n_x} \times \mathbb{R}^{m_x}$, describes the conditions where the transition from μ_1 to μ_2 occurs. It is represented as $\mathcal{G}(\{\mu_1, \mu_2\})$.
- *Reset Map*, $\mathcal{R} : \mathcal{E} \times \mathbb{R}^{n_x} \times \mathbb{R}^{m_x} \to \mathbb{R}^{n_x}$, means the jump of the state variable x. It is expressed as $\mathcal{R}(\{\mu_1, \mu_2\}, (x, u_x))$.

B. Notations

In this work, we use 0_{ij}, I_i and e_3 to denote the $i \times j$ zero matrix, the $i \times i$ identity matrix and $[0\ 0\ 1]^\top$. Also, we define a_i, $[a]$, $\dim(a)$, $A_{i,j}$, $A_{i:j,k:l}$ and $\mathcal{B}_\sigma(a)$ as the i-th element of a column vector a, the $so(3)$ operator representing the cross product $[a]b = a \times b$, the dimension of a, the (i,j)-th element a matrix A, the block matrix of A containing from (i,k)-th to (j,l)-th elements and the set $\{c \in \mathbb{R}^{\dim(a)} \mid \|c - a\| \leq \sigma\}$ where σ is a constant positive number. The Kronecker product is expressed as $\otimes$.

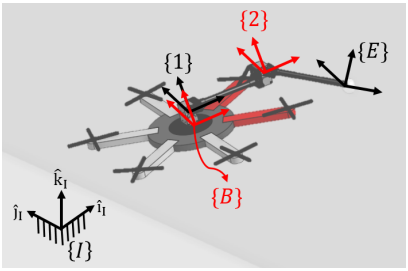

Fig. 2: The picture depicting an aerial manipulator perching on the wall connected by a spherical joint. The wall is aligned with $\hat{j}_I$-$\hat{k}_I$ plane, and the aerial manipulator pulls the plug out of the socket in -$\hat{i}_I$ direction.

As in Fig. 2, we denote the frame of the inertial coordinate, multirotor, 1st, 2nd servo motor and the end-effector by $\{I\}$, $\{B\}$, $\{1\}$, $\{2\}$ and $\{E\}$ respectively.

To express the state of an aerial manipulator, we define the generalized coordinate q as $[p_{IB}^\top\ \eta^\top\ \gamma^\top]^\top$ consisting of the position of the multirotor $p_{IB} \triangleq [p_x\ p_y\ p_z]^\top \in \mathbb{R}^3$, Euler angles $\eta \triangleq [\phi\ \theta\ \psi]^\top \in \mathbb{R}^3$ where ϕ, θ and ψ represent roll, pitch and yaw angles, and the angles of servo motors $\gamma \triangleq [\gamma_1\ \gamma_2]^\top \in \mathbb{R}^2$. Also, we let χ, r, x_q and x_r denote $[p_{IB}^\top\ \eta^\top]^\top$, $[\eta^\top\ \gamma^\top]^\top$, $[q^\top \dot{q}^\top]^\top$ and $[r^\top \dot{r}^\top]^\top$. To represent inputs, we use u_f and u to denote $[T\ \tau_b^\top\ \tau_\gamma^\top]^\top$ and $[T\ \tau_b^\top]^\top$ where T, τ_b and τ_γ mean a total thrust, moments with respect to $\hat{i}_B$, $\hat{j}_B$ and $\hat{k}_B$ and torque inputs exerted on the servo motors. We let $Q \in \mathbb{R}^{3\times3}$ denote a matrix which satisfies $\omega_{IB}^B = Q\dot{\eta}$ and the scalar g the gravitational acceleration. Moreover, we set a_d, $\hat{a}$ and $\bar{A}$ as a desired trajectory, an estimate of a and the nominal value of A.

We use m_b, m_1 and m_2 to denote mass of the multirotor, the 1st and the 2nd servo motor while diagonal matrices J_b, J_1, J_2 in $\mathbb{R}^{3\times3}$ are the moments of inertia of the corresponding components. Additionally, $J_E \in \mathbb{R}^{3\times3}$ means the moment of inertia of the end-effector.

C. Scenario

As in Fig. 2, the aerial manipulator tries to unplug in $-\hat{i}_I$ direction from the socket installed on the wall aligned with $\hat{j}_I$-$\hat{k}_I$ plane. After the plug is separated from the socket, the vehicle quickly stabilizes its attitude in a short time and maintains the hovering state.

III. HYBRID AUTOMATA OF AERIAL PLUG-PULLING

We construct the elements of the hybrid automata listed in Section II-A for the aerial manipulator pulling the plug.

A. Set of Operative Modes, $\mathcal{M}$ = {*WP, ST, FF*}

In WP (*wire-pulling*) mode, the aerial manipulator tries to unplug by pulling the wire in $-\hat{i}_I$ direction. In ST (*stabilizing*) mode, the vehicle quickly stabilizes its attitude immediately after the separation of the plug. In FF (*free-flight*) mode, the aerial manipulator returns to the original location and keeps the hovering state.

B. Domain Mappings, $\mathcal{D}(WP)$, $\mathcal{D}(ST)$ and $\mathcal{D}(FF)$

- $\mathcal{D}(WP) \triangleq \{(x_r, u_f) \in \mathbb{R}^{10} \times \mathbb{R}^6 \mid F_{E,1} < F_{TH}\}$ where F_E is the interaction force acting on the end-effector due to the friction between the plug and the socket and F_{TH} is the force limit up to which the plug can resist from separating.
- $\mathcal{D}(FF \ or \ ST) \triangleq \mathcal{V}_F - \mathcal{D}(WP)$ where $\mathcal{V}_F$ means an $\mathbb{R}^{16} \times \mathbb{R}^6$ space representing the flight envelope, i.e., all possible regions of the state and inputs for the flight experiment.

C. Flow Maps, $f(WP, x_r, u_f)$ and $f(ST \ or \ FF, x_q, u_f)$

1) WP mode: The derivation of $f(WP, x_r, u_f)$ is based on [1], but since the position of the end-effector is fixed, we newly derive it in the form of the Euler-Lagrange equation with $r = [\eta^\top \ \gamma^\top]^\top$ which fully describes the dynamics of the wire-pulling aerial manipulator.

First we express position and angular velocity as

$$\begin{aligned} &p_{IB} = p_{IE} - R_{IB}p_{BE}, \ p_{I1} = p_{IE} + R_{IB}p_{B1} - R_{IB}p_{BE}, \\ &p_{I2} = p_{IE} + R_{IB}p_{B2} - R_{IB}p_{BE}, \\ &\omega_{IB}^B = Q\dot{\eta}, \quad \omega_{I1}^1 = R_{B1}^\top(\omega_{IB}^B + \omega_{B1}^B), \\ &\omega_{I2}^2 = R_{b2}^\top(\omega_{IB}^b + \omega_{B2}^B), \quad \omega_{IE}^E = R_{BE}^\top(\omega_{IB}^B + \omega_{BE}^B). \end{aligned} \tag{1}$$

with the kinematic constraint $\dot{p}_{IE} = 0_{31}$ By substituting (1) into the derivation process presented in [1], an Euler-Lagrange equation of the wire-pulling aerial manipulator model can be derived. Then, the obtained equation of motion can be analyzed in the form of flow map as follows.

$$\ddot{r} = f(WP, x_r, u_f) = M_r^{-1}(-C_r - K_r + J_{ur}^T u_f + \tau_{e,r}) \tag{2}$$

where $M_r \in \mathbb{R}^{5\times5}$, $C_r \in \mathbb{R}^5$, $K_r \in \mathbb{R}^5$,

$$J_{ur} \triangleq \frac{\partial[\dot{p}_{IB}^{B\top} \ \omega_{IB}^{B\top} \ \dot{\gamma}^\top]^\top}{\partial r} \in \mathbb{R}^{6\times5},$$

and $\tau_{e,r}$ means the external disturbance applied to the wire-pulling aerial manipulator system. Thus, the variable x_r evolves in correspondence with (2).

2) ST and FF modes: The Euler-Lagrange equation for the multirotor equipped with the 2 DOF robotic arm is derived in [1]. Then, the flow map $f(ST \ or \ FF, x_q, u_q)$ can be derived as follows.

$$\begin{aligned} \ddot{q} &= f(ST \ or \ FF, x_q, u_q) \\ &= M_q^{-1}(-C_q - K_q + J_{uq}^T u_f + \tau_{e,q}) \end{aligned} \tag{3}$$

where $M_q \in \mathbb{R}^{8\times8}$, $C_q \in \mathbb{R}^8$, $K_q \in \mathbb{R}^8$, $J_{uq} \in \mathbb{R}^{6\times8}$, and $\tau_{e,q}$ means the external disturbance applied to the system in free flight.

D. Set of Edges, $\mathcal{E} = \{(WP, ST), (ST, FF)\}$

There would be only two possible edges in our scenario because the transition from ST or FF mode to WP mode does not occur unless the plug is attached to the socket again. Also, a change from FF to ST mode is impossible because the ST mode is primarily designed as an intermediate stage between the WP and FF modes.

E. Guard Mappings, $\mathcal{G}(\{WP, ST\})$ and $\mathcal{G}(\{ST, FF\})$

A transition from WP mode to ST mode occurs when the $\hat{i}_I$ element of F_E exceeds F_{TH}. Therefore, the guard map $\mathcal{G}(\{WP, ST\})$ is defined as $\{(x_r, u_f) \in \mathcal{D}(WP) \mid F_{E,1} = F_{TH}\}$. Also, since ($\phi_d$, θ_d) in the ST mode are user-defined values while they are computed from the user-defined values of (x_d, y_d) in the FF mode, an undesirable abrupt change in (ϕ_d, θ_d) would provoke a failure in attitude control. Therefore, the guard map $\mathcal{G}(\{ST, FF\})$ is defined as $\{(x_q, u_f) \in \mathcal{D}(ST) \mid \|\eta\| < \delta_\eta, \ t_{d,ST} \le t\}$ where δ_η is defined as the threshold of η for the mode change.

F. Reset maps, $\mathcal{R}(\{WP, ST\}, (x_r, u_f))$ and $\mathcal{R}(\{ST, FF\}, (x_q, u_f))$

If the operative mode changes from WP to ST, there would be jumps in x_q due to the sudden disappearance of the force exerted on the end-effector. However, since we cannot know the exact magnitude of the jumps in x_q, we denote it by x_q which satisfies $\dot{p}_{IE}(x_q) \neq 0_{31}$. Then, the reset map $\mathcal{R}(\{WP, ST\}, (x_q, u_f))$ is expressed as $\{x_q^+ \in \mathcal{D}_{x_q^+}(ST) \mid \dot{p}_{IE}(x_q^+) \neq 0_{31}$ where $x_r \in \mathcal{D}_{x_r}(WP)\}$. On the other hand, the change from ST to FF does not entail any jump in x_q because they evolve under the same dynamics. Therefore, the reset map $\mathcal{R}(\{ST, FF\}, (x_q, u_f))$ can be derived as $\{x_q^+ \in \mathcal{D}_{x_q^+}(FF) \mid x_q^+ = x_q$ where $x_q \in \mathcal{D}_{x_q}(ST)\}$.

IV. TRAJECTORY GENERATION AND CONTROLLER DESIGN

A. Trajectory Generation

It is assumed that γ and $\dot{\gamma}$ exactly follow γ_d and $\dot{\gamma}_d$ respectively and the desired values that are not defined at each mode are set to be the same as the current values.

1) WP mode: In this mode, the aerial manipulator tries to tilt its body with respect to $-\hat{j}_B$ in order to exercise a pulling force to the socket. Therefore, $\eta_d(t)$ is given as below,

$$\eta_d(t) = \begin{cases} [0 \ \ -\theta_m(\frac{t - t_{0,WP}}{t_{d,WP} - t_{0,WP}}) \ 0]^\top, & t_{0,WP} \le t < t_{d,WP} \\ 0_{31}, & t_{d,WP} \le t \end{cases} \tag{4}$$

where θ_m means the maximum absolute value of the pitch angle. It prevents a sudden transition to ST mode by gradually tilting the vehicle's body.

2) ST mode: This mode is proposed for compensating the overshoot invoked by the transition of the dynamical model and avoiding an abrupt change in $\phi_d(t)$ and $\theta_d(t)$. In order to simultaneously minimize the overshoot and make ϕ and θ close to zero, the time interval $[t_{0,ST}, t_{d,ST})$ needs to be reasonably small. Therefore, $p_{z,d}(t)$ and $\eta_d(t)$ are set as

$$p_{z,d}(t) = p_z(t_{0,ST})$$

$$\eta_d(t) = \begin{cases} c_2 t^2 + c_1 t + c_0, & t_{0,ST} \le t < t_{d,ST} \\ 0_{31}, & t_{d,ST} \le t \end{cases} \tag{5}$$

where coefficients c_0, c_1 and c_2 satisfy the conditions $\eta_d(t_{0,ST}) = \eta(t_{0,ST})$, $\dot{\eta}_d(t_{0,ST}) = \dot{\eta}(t_{0,ST})$ and $\eta_d(t_{d,ST}) = 0_{31}$.

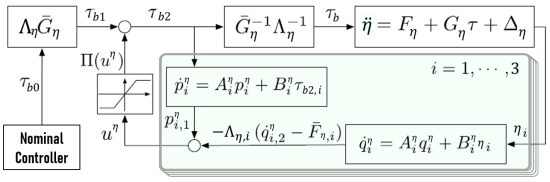

Fig. 3: The DOB structure of WP mode for compensating the model discrepancy Δ_η between (8) and (9).

3) FF mode: In FF mode, p_{Ib} and ψ are set to fly back to the original position as follows:

$$p_{Ib,d}(t) = p_{Ib}(t_{0,WP}),\ \psi_d(t) = \psi(t_{0,WP}) \tag{6}$$

B. Nominal Model for Each Mode

Servo motors are usually controlled by the given desired position, not torque. Therefore, the equations of motion that eliminate the term τ_γ are derived for each model.

1) WP mode: In (2), J_{ur} is computed as

$$J_{ur}^\top = \begin{bmatrix} J_{T\eta}^\top & Q^\top & 0_{32} \\ J_{T\gamma}^\top & 0_{23} & I_2 \end{bmatrix},\ J_{T_\eta} \in \mathbb{R}^{1\times 3},\ J_{T_\gamma} \in \mathbb{R}^{1\times 2}. \tag{7}$$

Therefore, the model with respect to η is obtained with known values T, γ, $\dot{\gamma}$ and an observable value $\ddot{\gamma}$ as follows.

$$\ddot{\eta} = F_\eta + G_\eta \tau_b \tag{8}$$

where

$$\begin{aligned} F_\eta &\triangleq M_\eta^{-1}\{-C_\eta - K_\eta - M_{\eta\gamma}\ddot{\gamma} - J_{T_\eta}^\top T - \tau_{e,r}\} \\ G_\eta &\triangleq M_\eta^{-1} Q^\top \end{aligned}$$

with block matrices $M_\eta = M_{r,1:3,1:3}$, $M_{\eta\gamma} = M_{r,1:3,4:5}$, $C_\eta = C_{r,1:3,1}$ and $G_\eta = G_{r,1:3,1}$. Then based on this, the nominal model for the WP mode can be obtained as follows.

$$\ddot{\eta} = \bar{F}_\eta + \bar{G}_\eta \tau_{b0} \tag{9}$$

where

$$\begin{aligned} \bar{F}_\eta &\triangleq \bar{M}_\eta^{-1}\{-\bar{C}_\eta - \bar{K}_\eta - \bar{M}_{\eta\gamma}\ddot{\bar{\gamma}} - \bar{J}_{T_\eta}^\top T\} \\ \bar{G}_\eta &\triangleq \bar{J}_b^{-1} Q^\top \end{aligned} \tag{10}$$

with the nominal input $u_0 = [T\ \tau_{b0}^\top]^\top$. The total thrust T is calculated in the DOB controller introduced in [17].

2) ST and FF mode: The nominal model for ST and FF mode is derived in [17] as below.

$$\ddot{q}_u = \bar{G}_u \Phi_0, \qquad \ddot{q}_f = \bar{F}_f + \bar{G}_f u_0 \tag{11}$$

where q_u and q_f mean the center of mass of $[p_x\ p_y]^\top$ and $[p_z\ \eta^\top]^\top$ respectively. The other notations are defined in [17].

C. Controller Design

1) WP mode: If we design the nominal input τ_{b0} to make the solution of (9) adequately follows η_d, the compensation of model discrepancy, $\Delta_\eta \triangleq (F_\eta - \bar{F}_\eta) + (G_\eta\tau_b - \bar{G}_\eta\tau_{b0})$, is conducted by the DOB structure presented in [10]. The overall diagram is shown in Fig. 3 and the detailed DOB control law is formulated as below.

$$\begin{aligned} &\dot{q}_i^\eta = A_{\eta,i} q_i^\eta + B_{\eta,i}\eta_i, \quad \dot{p}_i^\eta = A_{\eta,i} p_i^\eta + B_{\eta,i}\tau_{b2,i} \\ &u_i^\eta = p_{i,1}^\eta - \sum_{j=1}^{3} \Lambda_{\eta,i,j}(\dot{q}_{j,2}^\eta - \bar{F}_{\eta,j}), \quad \tau_{b1} = \Lambda_\eta \bar{G}_\eta \tau_{b0} \\ &\tau_{b2} = \Lambda_\eta \bar{G}_\eta \tau_{b0} + \Pi_\eta(u^\eta),\ \tau_b = \tau_{b0} + (\Lambda_\eta \bar{G}_\eta)^{-1}\Pi_\eta(u^\eta) \end{aligned} \tag{12}$$

where $q^\eta = [q_{1,1}^\eta\ q_{1,2}^\eta\ \cdots\ q_{3,2}^\eta]^\top$, $p^\eta = [p_{1,1}^\eta\ p_{1,2}^\eta\ \cdots\ p_{3,2}^\eta]^\top$, $u^\eta = [u_1^\eta\ u_2^\eta\ u_3^\eta]^\top$ and

$$\begin{aligned} A_i^\eta &= \begin{bmatrix} 0 & 1 \\ -a_{i,0}^\eta/\epsilon_\eta^2 & -a_{i,1}^\eta/\epsilon_\eta \end{bmatrix}, \quad B_i^\eta = \begin{bmatrix} 0 \\ a_{i,0}^\eta/\epsilon_\eta^2 \end{bmatrix} \\ \Lambda_\eta &= \bar{J}_b^{(1/2)} Q \in \mathbb{R}^{3\times 3} \end{aligned}$$

with the positive constants $a_{i,0}^\eta$, $a_{i,1}^\eta$ and the small positive constant ϵ_η. In this DOB structure, we use a saturation function Π_η defined with the conditions below.

- Π_η: $\mathbb{R}^3 \Rightarrow \mathbb{R}^3$ is a globally bounded $\mathcal{C}^1$ function.
- $\Pi_\eta(u^\eta) = u^\eta$ for $\forall u^\eta \in S_{u^\eta}$ where $S_{u^\eta} \triangleq \{u^\eta \in \mathbb{R}^{3\times 1} \mid u^\eta = \Lambda_\eta \bar{G}_\eta G_\eta^{-1}(\bar{F}_\eta - F_\eta + (\bar{G}_\eta - G_\eta)\tau_{b0} - \Delta_\eta)\}$.
- $\|\partial\Pi_\eta(u^\eta)/\partial u^\eta\| \le 1$ for $\forall u^\eta \in \mathbb{R}^{3\times 1}$

From the conditions above, the quasi-steady state range of u^η satisfies the equation $u_i^\eta = p_{i,1}^\eta - \sum_{j=1}^3 \Lambda_{\eta,i,j}(\dot{q}_{j,2}^\eta - \bar{F}_{\eta,j})$ while avoiding the saturation [10].

2) ST mode: For the ST mode, we only apply the DOB structure for the fully-actuated system introduced in [18].

3) FF mode: We will utilize the same controller presented in [17] for the FF mode.

V. STABILITY AND ROBUSTNESS ANALYSIS

In this section, an analysis of the stability and robustness will be presented. During the analysis, the term *maneuver* which means $[x_q^\top u_f^\top]^\top$ in a particular mode will be used. v_μ and $\bar{v}_\mu^N$ mean the solution from the actual flow map and the nominal flow map. Additionally, trv_μ is defined as a set including all values of v_μ in the given time interval.

A. Preliminary Definitions for the Analysis on Hybrid Automata

Definition 1 (σ-robust μ_1-single maneuver in $[t_{0,\mu_1}, t_1)$)**.** For $\sigma > 0$, $\mu_1 \in \mathcal{M}$ and $0 < t_1$, a maneuver $\bar{v}_{\mu_1}^N \in [t_{0,\mu_1}, t_1)_{\mu_1}$ satisfies

$$\text{tr}\ \bar{v}_{\mu_1}^N \bigcap \Big(\bigcup_{\{\mu_1,\mu'\}\in\mathcal{E}} \mathcal{G}(\{\mu_1,\mu'\}) + \mathcal{B}_\sigma \Big) = \varnothing. \tag{13}$$

Here, $[t_{0,\mu}, t_1)_\mu$ means the time interval where $\bar{v}_{WP}^N$ evolves in the mode μ within $[t_{0,\mu}, t_1)$.

Definition 2 (σ-robust $\mu_1 \mapsto \mu_2$ approach maneuver in $[t_{0,\mu_1}, t_1)$)**.** For $\sigma > 0$, $\mu_1, \mu_2 \in \mathcal{M}$ and $t_{0,\mu_1} \le t_1$, a maneuver $\bar{v}_{\mu_1}^N \in [t_{0,\mu_1}, T]_{\mu_1}$ satisfies

- tr $\bar{v}_{\mu_1}^N \bigcap \big(\bigcup_{\{\mu_1,\mu_2'\}\in\mathcal{E}-\{\mu_1,\mu_2\}} \mathcal{G}(\{\mu_1,\mu_2'\}) + \mathcal{B}_\sigma \big) = \varnothing$ and $\mathcal{B}_\sigma(\bar{v}_{\mu_1}^N) \subset \mathcal{G}(\{\mu_1,\mu_2\})$
- Let S^{μ_1} and $S^{\mu_1\to\mu_2}$ be compact sets defined as $S^{\mu_1} \triangleq (\text{tr}\bar{v}_{\mu_1}^N + \mathcal{B}_\sigma) \cap \mathcal{G}(\{\mu_1,\mu_2\})$ and

$$\begin{aligned} &S^{\mu_1\to\mu_2} \triangleq \{x_q^+ \in \mathcal{D}_{x_q}(\mu_2) \mid x_q^+ \in \\ &\mathcal{R}(\{\mu_1,\mu_2\}, (x_q,u_f) \text{ for some } (x_q,u_f) \in S^{\mu_1}\} \end{aligned} \tag{14}$$

Then, for any $x_q^+ \in S^{\mu_1 \mapsto \mu_2}$ there exists u_f^+ such that

$$(x_q^+, u_f^+) \notin \bigcup_{\{\mu_2, \mu_2'\} \in \mathcal{E}} \mathcal{G}(\{\mu_2, \mu_2'\}) + \mathcal{B}_\sigma. \tag{15}$$

Definition 3 ((σ, δ_σ)-robust $S^{\mu_1 \mapsto \mu_2}$ coverage set, $\mathcal{C}_{\delta_\sigma}^{\mu_1 \mapsto \mu_2}$)**.** A set of N_{δ_σ} elements $x_{q,1}, ..., x_{q,N_{\delta_\sigma}} \in \mathcal{D}_{x_q}(\mu_2)$ which satisfies

$$S^{\mu_1 \mapsto \mu_2} \subset \bigcup_{j \in \{0, ..., N_{\delta_\sigma}\}} \mathcal{B}_{\delta_\sigma}(x_{q,j}). \tag{16}$$

Definition 4 ((σ, δ_σ)-robust $\mu_1 \mapsto \mu_2$ transition maneuver)**.** For $\sigma > 0$, $\delta_\sigma > 0$, $\mu_1, \mu_2 \in \mathcal{M}$ and $t_{0,\mu_1} < t_1$, $\bar{v}_{\mu_1}^N$ which is a union of a σ-robust $\mu_1 \mapsto \mu_2$ approach maneuver before the switching time $T \in (t_{0,\mu_1}, t_1)$ and of a set of N_{δ_σ} σ-robust single maneuvers after transition with the property $v_{\mu_2,j} \in \mathcal{C}_{\delta_\sigma}^{\mu_1 \mapsto \mu_2}, \forall j \in \{1, ..., N_{\delta_\sigma}\}$.

B. Robustness of the Nominal maneuver

With the assumption that x_q of the nominal maneuver $\bar{v}_\mu^N$ adequately follows $x_{q,d}$ defined through (4) – (6), we analyze the characteristics of the nominal maneuver.

1) (σ, δ_σ)-robust $WP \mapsto ST$ transition maneuver: With the assumption that the aerial manipulator is in a quasi-equilibrium state while perching on the wall, the pulling force $F_{E,1}$ is equal to $-T \sin\theta$ [4]. Thus, $F_{E,1}$ increases with the gradually decreasing trajectory of θ as generated in (4). As a result, $\bar{v}_{WP}^N$ does not reach $\mathcal{G}\{(WP, ST)\} + \mathcal{B}_\sigma$ before $F_{E,1}$ closely approaches F_{TH}. Moreover, as depicted in Fig. 4a, there is no possibility of a transition from WP to FF mode because $\mathcal{G}\{(WP, FF)\}$ is defined as $\varnothing$. Therefore, the maneuver $\bar{v}_{WP}^N$ is proved to be a σ-robust WP-single maneuver in $[t_{0,WP}, t_{0,ST})$.

$\bar{v}_{WP}^N$ can also become a σ-robust $WP \mapsto ST$ approach maneuver when there exists a time instant that a change from WP to ST occurs in a finite time. Thanks to the relation that $F_{E,1}$ equals to $-T \sin\theta$, we can easily find a sufficient condition $0 < F_{TH} < T_m \sin\theta_m$ where T_m means the maximum value of T. The inequality above infers that $F_{E,1}$ can reach F_{TH} with the given trajectory of θ. Additionally, since the direct change from WP to FF mode never occurs as mentioned above, the claim that $\bar{v}_{WP}^N$ is a robust approach maneuver is proved.

After the transition from WP to ST mode, the reset map of $\bar{v}_{WP}^N$ is uncertain. However, we can avoid the situation where the value of $\mathcal{R}(\{(WP, ST)\}, (x_r(t_{0,ST}), u_f(t_{0,ST})))$ becomes an element of $\mathcal{D}(FF)$ the switch from ST to FF does not occur before the time reaches the value of $t_{d,ST}$ by the condition $t_{d,ST} < t$ in $\mathcal{G}\{(ST, FF)\}$. Therefore, a maneuver $\bar{v}_{WP}^N$ turns out to be a σ-robust ST-single maneuver in $[t_{0,WP}, t_{0,ST})$ after the mode transition. From the analyses above, the union of $\mathrm{tr}\bar{v}_{WP}^N$ and $\mathrm{tr}\bar{v}_{ST}^N$ is proved to be a (σ, δ_σ)-robust $WP \mapsto ST$ transition maneuver.

2) (σ, δ_σ)-robust $ST \mapsto FF$ transition maneuver: As proved in the previous section, the maneuver $\bar{v}_{ST}^N$ is a σ-robust ST-single maneuver in $[t_{0,ST}, t_{0,FF})$. Also, there must be a change from ST to FF mode in a finite time since η_d defined in ST mode reaches 0_{31} when t reaches $t_{d,ST}$. Also, since the transition from ST to WP mode is impossible, $\bar{v}_{ST}^N$ also turns out to be a σ-robust $ST \mapsto FF$ approach maneuver in $[t_{0,ST}, t_{0,FF})$.

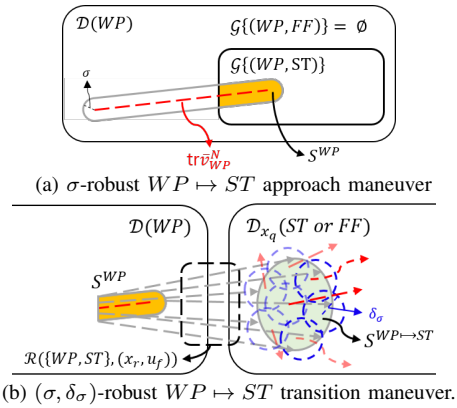

(a) σ-robust $WP \mapsto ST$ approach maneuver

(b) (σ, δ_σ)-robust $WP \mapsto ST$ transition maneuver.

Fig. 4: Venn diagram demonstrating hybrid automata in WP and ST modes. (a) A red dashed line means the trace of the nominal maneuver in WP mode. A yellow region describes the set of possible maneuvers which can provoke a change from WP to ST mode. (b) A green region expresses the set of reset maps from the maneuvers initiating from the yellow region. Blue dashed circles are centered in N_{δ_σ} elements in $C_{\delta_\sigma}^{WP \mapsto ST}$ and have the radius δ_σ. Red dashed arrows describe N_{δ_σ} maneuvers starting from $x_{q,j}$ where $j = 1, ..., N_{\delta_\sigma}$. Following Definition 3, all the blue dashed circles cover the green region.

Accordingly, the property that (FF, ST) and (FF, WP) are not the elements of $\mathcal{E}$ also guarantees that a maneuver $\bar{v}_{FF}^N$ is a σ-robust FF-single maneuver in $[t_{0,FF}, t_{d,FF})$. Thus, it is proved that the union of $\mathrm{tr}\bar{v}_{ST}^N$ and $\mathrm{tr}\bar{v}_{FF}^N$ becomes a (σ, δ_σ)-robust $ST \mapsto FF$ transition maneuver.

C. Analysis on Stability and Robustness at Each Mode

1) Wire-pulling mode: Prior to formulating a theorem about the stability and robustness of the WP mode, there need some remarks and assumptions as below.

Remark 1. *η_d, $\dot{\eta}_d$, $\ddot{\eta}_d$ are continuous and bounded in $\mathcal{C}^2$. In addition, let $\eta_d \in S_{\eta_d}$ where S_{η_d} is a known compact set.*

Assumption 1. *Let $\bar{\eta}^N(t)$ be the nominal solution of (9). For given η_d, the solution $\bar{\eta}^N(t)$ evolves in a bounded set $\mathcal{U}_\eta$ if the initial condition $\bar{\eta}^N(0)$ is in a compact set $S_\eta \subset \mathcal{U}_\eta$, and $\bar{\eta}^N(t) - \eta_d(t)$ initiated in S_η is locally asymptotically stable.*

Assumption 2. *According to [18], the aerodynamic effects, such as drag or buoyancy forces, are negligible in a near hovering condition due to the small size of the multirotors. Also, frictional torque and force applied on the end-effector are at least $\mathcal{C}^2$ and bounded in $\mathcal{U}_\eta$ because they are functions of r and $\dot{r}$.*

Remark 2. The terms M_r, $\bar{M}_r$, $M_{\eta\gamma}\ddot{\gamma}$, $\bar{M}_{\eta\gamma}\ddot{\bar{\gamma}}$, C_r, $\bar{C}_r$, G_r, $\bar{G}_r$, J_{ur} and $\bar{J}_{ur}$ are vectors and matrices which consist of r, $\dot{r}$ and $\ddot{r}$. Thus, these terms are at least $\mathcal{C}^2$ and bounded in $\mathcal{U}_\eta$. Moreover, by the assumption 2, $\tau_{e,r}$ is also a vector that is $\mathcal{C}^2$ and bounded in $\mathcal{U}_\eta$. Since F_η, $\bar{F}_\eta$, G_η and $\bar{G}_\eta$ have the terms described above, vectors and matrices shown in (9) are all at least $\mathcal{C}^2$ and bounded in $\mathcal{U}_\eta$.

Then finally, from the assumptions and remarks stated

above, we can formulate a theorem on the relationship similar to the theorem introduced in [17] and prove it.

Theorem 1. *Let S_{qp}^{η} be a compact set for the initial condition $[q^{\eta}(0)^{\top}\ p^{\eta}(0)^{\top}]^{\top}$, and $\bar{S}_{\eta}$ be a compact set smaller than S_{η}. For a given $\sigma > 0$, there exists ϵ_{η}^{*} such that, for each $0 < \epsilon_{\eta} < \epsilon_{\eta}^{*}$, the solution of (9), $[\bar{\eta}^{N}(t)^{\top}\dot{\eta}^{N}(t)^{\top}\bar{\tau}_{b0}^{N}(t)^{\top}]^{\top}$, and that of (8), $[\eta(t)^{\top}\dot{\eta}^{N}(t)^{\top}\tau_{b0}(t)^{\top}]^{\top}$, initiated at $[\eta(0)^{\top}\dot{\eta}(t)^{\top}\tau_{b0}(t)^{\top}q^{\eta}(0)^{\top}p^{\eta}(0)^{\top}]^{\top} \in \bar{S}_{\eta} \times S_{qp}^{\eta}$ satisfies*

$$\|[\eta(t)^{\top}\dot{\eta}(t)^{\top}\tau_{b0}(t)^{\top}] - [\bar{\eta}^{N}(t)^{\top}\dot{\eta}^{N}(t)^{\top}\bar{\tau}_{b0}^{N}(t)^{\top}]\| \leq \sigma,\ \forall t \geq 0$$

if we set the initial conditions for both dynamic models identical, $[\bar{\eta}^{N}(0)^{\top}\dot{\eta}^{N}(0)^{\top}\bar{\tau}_{b0}^{N}(0)^{\top}]^{\top} = [\eta(0)^{\top}\dot{\eta}(0)^{\top}\tau_{b0}(0)^{\top}]^{\top}$.

Proof: Proof of this theorem will follow the procedure introduced in [18]. ■

Lemma 1. *With fast variables $\xi^{\eta} \triangleq [\xi_1^{\eta T}\ \xi_2^{\eta T}\ \xi_3^{\eta T}]^{\top}$ and $\zeta^{\eta} \triangleq [\zeta_1^{\eta T}\ \zeta_2^{\eta T}\ \zeta_3^{\eta T}]^{\top} \in \mathbb{R}^{6\times 1}$ defined as*

$$\xi_i^{\eta} = \begin{bmatrix}\xi_{i,1}^{\eta}\\ \xi_{i,2}^{\eta}\end{bmatrix} = \begin{bmatrix}\frac{1}{\epsilon_{\eta}}q_{i,1}^{\eta} + \frac{a_{i,1}^{\eta}}{a_{i,0}^{\eta}}q_{i,2}^{\eta} - \frac{1}{\epsilon_{\eta}}\eta_i\\ q_{i,2}^{\eta} - \dot{\eta}_i\end{bmatrix} \in \mathbb{R}^{2\times 1}$$
$$\zeta_i^{\eta} = \begin{bmatrix}\zeta_{i,1}^{\eta}\\ \zeta_{i,2}^{\eta}\end{bmatrix} = \begin{bmatrix}p_{i,1}^{\eta} - \Lambda_i\dot{q}_{i,2}^{\eta}\\ \epsilon_{\eta}(\dot{p}_{i,1}^{\eta} - \ddot{q}_{i,2}^{\eta})\end{bmatrix} \in \mathbb{R}^{2\times 1}, \tag{17}$$

the closed-loop system of the actual model describing wire-pulling mode can be rearranged in the standard singular perturbation form as follows.

$$\begin{aligned}\ddot{\eta} &= F_{\eta} + G_{\eta}(\tau_{b0} + (\Lambda_{\eta}\bar{G}_{\eta})^{-1}\Pi(u^{\eta})) + \Delta_{\eta}\\ \epsilon_{\eta}\dot{\xi}_i^{\eta} &= A_{\xi,i}^{\eta}\xi_i^{\eta} - \epsilon_{\eta}B_2^{\eta}(F_{\eta,i} + G_{\eta,i}\tau_b + \Delta_{\eta,i})\\ \epsilon_{\eta}\dot{\zeta}_i^{\eta} &= A_{\zeta,i}^{\eta}\zeta_i^{\eta} + B_2^{\eta}a_{i,0}^{\eta}(\tau_{b2,i}\\ &\quad - \sum_{j=1}^{3}\Lambda_{\eta,i,j}(F_{\eta,j} + G_{\eta,j}\tau_b + \Delta_{\eta,j}))\end{aligned} \tag{18}$$

where $B_2^{\eta} \triangleq [0\ 1]^{\top}$ and

$$A_{\xi,i}^{\eta} \triangleq \begin{bmatrix}-a_{i,1}^{\eta} & 1\\ -a_{i,0}^{\eta} & 0\end{bmatrix},\quad A_{\zeta,i}^{\eta} \triangleq \begin{bmatrix}0 & 1\\ -a_{i,0}^{\eta} & -a_{i,1}^{\eta}\end{bmatrix}.$$

Proof: The derivation of Lemma 1 is based on [19, Appendix A]. ■

To obtain the reduced model of (8), the quasi-states of (ξ^{η}, ζ^{η}) are obtained as follows by setting $\epsilon_{\eta} = 0$.

$$\begin{aligned}&\xi^{\eta,*} = 0_{61}\\ &\zeta_{[1]}^{\eta,*} = \tau_{b2} - \Lambda_{\eta}(F_{\eta} + G_{\eta}\tau_b + \Delta_{\eta}),\ \zeta_{[2]}^{\eta,*} = 0_{31}\end{aligned} \tag{19}$$

where $\zeta_{[1]}^{\eta,*} \triangleq [\zeta_{1,1}^{\eta,*}\ \zeta_{2,1}^{\eta,*}\ \zeta_{3,1}^{\eta,*}]^{\top}$ and $\zeta_{[2]}^{\eta,*} \triangleq [\zeta_{1,2}^{\eta,*}\ \zeta_{2,2}^{\eta,*}\ \zeta_{3,2}^{\eta,*}]^{\top}$.

Since u^{η} turns out to be equal to $\zeta_{[1]}^{\eta} + \Lambda_{\eta}\bar{F}_{\eta}$ from (12) and (17), an equation on $u^{\eta*}$ can be formulated as

$$\begin{aligned}u^{\eta*} - \Lambda_{\eta}((\bar{F}_{\eta} - F_{\eta}) + (\bar{G}_{\eta} - G_{\eta})\tau_{b0} - \Delta_{\eta})\\ - (I_3 - \Lambda_{\eta}G_{\eta}\bar{G}_{\eta}^{-1}\Lambda_{\eta}^{-1})\Pi_{\eta}(u^{\eta*}) = 0_{31}.\end{aligned} \tag{20}$$

Moreover, since $u^{\eta*} \in S_{u^{\eta}}$, $\Pi_{\eta}(u^{\eta*})$ equals $u^{\eta*}$. Therefore, an explicit expression for $u^{\eta*}$ is obtained as follows.

$$u^{\eta*} = \Lambda_{\eta}\bar{G}_{\eta}G_{\eta}^{-1}(\bar{F}_{\eta} - F_{\eta} + (\bar{G}_{\eta} - G_{\eta})\tau_{b0} - \Delta_{\eta}) \tag{21}$$

The next step is to show that the only solution for (20) is (21). Thus, we declare a function $\Gamma_{\eta}(\delta)$ which replaces $u^{\eta*}$ in (20) with $u^{\eta*} + \delta$ as below.

$$\begin{aligned}\Gamma_{\eta}(\delta) \triangleq& u^{\eta*} + \delta - \Lambda_{\eta}((\bar{F}_{\eta} - F_{\eta}) + (\bar{G}_{\eta} - G_{\eta})\tau_{b0} - \Delta_{\eta})\\ &- (I_3 - \Lambda_{\eta}G_{\eta}\bar{G}_{\eta}^{-1}\Lambda_{\eta}^{-1})\Pi_{\eta}(u^{\eta*} + \delta)\\ =&\delta + (\Lambda_{\eta}G_{\eta}\bar{G}_{\eta}^{-1}\Lambda_{\eta}^{-1} - I_3)(\Pi_{\eta}(u^{\eta*} + \delta) - \Pi_{\eta}(u^{\eta*})).\end{aligned}$$

Lemma 2. *With the assumption that $\eta \in \mathcal{U}_{\eta}$, $\Gamma_{\eta}(\delta)$ belongs to the sector $[1-\kappa, 1+\kappa]$ with $0 < \kappa < 1$. Then accordingly, $\delta = 0_{31}$ is the unique solution of $\Gamma_{\eta}(\delta) = 0_{31}$.*

Proof: From the definition of $\Gamma_{\eta}(\delta)$, the following inequality is derived.

$$|\Gamma_{\eta}(\delta) - \delta| \leq \|I_3 - \Lambda_{\eta}G_{\eta}\bar{G}_{\eta}^{-1}\Lambda_{\eta}^{-1}\|\|\Pi_{\eta}(u^{\eta*} + \delta) - \Pi_{\eta}(u^{\eta*})|$$

Since $\|\partial\Pi_{\eta}(u^{\eta})/\partial u^{\eta}\| \leq 1$, the inequality above is transformed into

$$|\Gamma_{\eta}(\delta) - \delta| \leq \|I_3 - \Lambda_{\eta}G_{\eta}\bar{G}_{\eta}^{-1}\Lambda_{\eta}^{-1}\||\delta|.$$

Based on (1) and the relation $\dot{R}_{IB} = R_{IB}[\omega_{IB}^{B}]$, if $\theta \in (-\frac{\pi}{2}, \frac{\pi}{2})$, $M_{\eta}^{*} \triangleq Q^{-\top}M_{\eta}Q^{-1}$ is organized as follows.

$$\begin{aligned}M_{\eta}^{*} =& m_b[R_{Ib}\hat{p}_{bE}]^{\top}[R_{Ib}\hat{p}_{bE}] + m_1[R_{I1}\hat{p}_{1E}^{b}]^{\top}\\ &\times [R_{I1}\hat{p}_{1E}^{b}] + m_2[R_{I2}\hat{p}_{2E}^{b}]^{\top}[R_{I2}\hat{p}_{2E}^{b}] + J_b\\ &+ R_{b1}^{\top}J_1R_{b1} + R_{b2}^{\top}J_2R_{b2} + R_{bE}^{\top}J_ER_{bE}\end{aligned} \tag{22}$$

If we set $\bar{J}_b < J_b$, we can formulate the inequality below by substituting (10) and $\Lambda_{\eta} = \bar{J}_b^{(1/2)}Q$ since $J_b < M_{\eta}^{*}$.

$$\|I_3 - \Lambda_{\eta}G_{\eta}\bar{G}_{\eta}^{-1}\Lambda_{\eta}^{-1}\| = \|I_3 - \bar{J}_b^{\frac{1}{2}}M_{\eta}^{*-1}\bar{J}_b^{\frac{1}{2}}\| < 1. \tag{23}$$

Thus, $|\Gamma_{\eta}(\delta) - \delta|$ turns out to be smaller than $|\delta|$ and there exists $\kappa \in (0, 1)$ such that $\Gamma_{\eta}(\delta)$ belongs to the sector [1 - κ, 1 + κ]. Accordingly, it is shown that the only solution of $\Gamma_{\eta}(\delta) = 0_{31}$ is $\delta = 0_{31}$. ■

To prove that the fast dynamic system in Lemma 1 is exponentially stable, we derive 1st order differential equations for $\tilde{\xi}^{\eta} \triangleq \xi^{\eta} - \xi^{\eta*}$ and $\tilde{\zeta}^{\eta} \triangleq \zeta^{\eta} - \zeta^{\eta*}$ as

$$\begin{aligned}\epsilon_{\eta}\dot{\tilde{\xi}}^{\eta} =& A_{\xi}^{\eta}\tilde{\xi}^{\eta} - \epsilon_{\eta}B_2^{\eta}\{F_{\eta} + G_{\eta}\tau_{b0} + G_{\eta}\bar{G}_{\eta}^{-1}\Lambda_{\eta}^{-1}\\ &\times \Pi_{\eta}(\zeta_{[1]}^{\eta*} + \zeta_{[1]}^{\eta} + \bar{F}_{\eta}) + \Delta_{\eta}\}\\ \epsilon_{\eta}\dot{\tilde{\zeta}}^{\eta} =& A_{\zeta}^{\eta}\tilde{\zeta}^{\eta} - B_2^{\eta}a_0^{\eta}\Gamma_{\eta}(\tilde{\zeta}_{[1]}^{\eta}) - \epsilon_{\eta}B_1^{\eta}\dot{\zeta}_{[1]}^{\eta*}\end{aligned} \tag{24}$$

where $\tilde{\zeta}_{[1]}^{\eta} \triangleq \zeta_{[1]}^{\eta} - \zeta_{[1]}^{\eta*}$, $A_{\zeta}^{\eta} \triangleq \mathtt{blkdiag}\{A_1^{\eta}, A_2^{\eta}, A_3^{\eta}\}$, $B_1^{\eta} \triangleq I_3 \otimes [1\ 0]^{\top}$, $B_2^{\eta} \triangleq I_3 \otimes [0\ 1]^{\top}$, $a_0^{\eta} \triangleq \mathtt{diag}\{a_{1,0}^{\eta}, a_{2,0}^{\eta}, a_{3,0}^{\eta}\}$ and $A_{\tilde{\zeta}}^{\eta} \triangleq \mathtt{blkdiag}\{A_{\tilde{\zeta},1}^{\eta}, A_{\tilde{\zeta},2}^{\eta}, A_{\tilde{\zeta},3}^{\eta}\}$ with $A_{\tilde{\zeta},i}^{\eta} \triangleq \begin{bmatrix}0 & 1\\ 0 & -a_{i,1}^{\eta}\end{bmatrix}$.

Remark 3. Since $\|\Lambda_{\eta}G_{\eta}\bar{G}_{\eta}^{-1}\Lambda_{\eta}^{-1} - I_3\| \leq \kappa < 1$, the given inequality

$$\begin{aligned}&|\Lambda_{\eta}G_{\eta}\bar{G}_{\eta}^{-1}\Lambda_{\eta}^{-1}v|^2\\ &\quad < (\Lambda_{\eta}G_{\eta}\bar{G}_{\eta}^{-1}\Lambda_{\eta}^{-1}v)^{\top}v + v^{\top}(\Lambda_{\eta}G_{\eta}\bar{G}_{\eta}^{-1}\Lambda_{\eta}^{-1}v)\end{aligned}$$

holds $\forall v \neq 0_{31}$. If there exists $\bar{v} \neq 0_{31}$ satisfying $\Lambda_{\eta}G_{\eta}\bar{G}_{\eta}^{-1}\Lambda_{\eta}^{-1}\bar{v} = 0_{31}$, it becomes contrary to the inequality

above. Therefore, $\Lambda_\eta G_\eta \bar{G}_\eta^{-1} \Lambda_\eta^{-1}$ is an invertible matrix. Accordingly, since G_η is not singular, $\|\bar{G}_\eta^{-1}\|$ is bounded. Moreover, since $\|\dot{G}_\eta^{-1}\| \leq \|G_\eta^{-1}\| \|\dot{G}_\eta\| \|G_\eta^{-1}\|$ holds and $(\bar{G}_\eta^{-1}, \dot{\bar{G}}_\eta^{-1})$ are bounded in $\mathcal{U}_\eta$ based on the relationship $\bar{G}_\eta = \bar{J}_b^{-1} Q^T$, $\|\dot{G}_\eta\|$ is also bounded.

Remark 4. Since the initial condition in Theorem 1 is $[\bar{\eta}^N(0)^\top \ \dot{\bar{\eta}}^N(0)^\top \ \bar{\tau}_{b0}^N(0)^\top]^\top = [\eta(0)^\top \ \dot{\eta}(0)^\top \ \tau_{b0}(0)^\top]^\top$ and η is bounded due to Remark 2 and the definition of Π_η, there exists $T_1 > 0$ such that $[\eta(t)^\top \tau_{b0}^\top]^\top$ remains in $\mathcal{U}_\eta$ for $t \in [0 \ T_1]$. Also, there exists $T_2 > 0$ such that $|[\eta(0)^\top \ \dot{\eta}(0)^\top \ \tau_{b0}(0)^\top]^\top - [\bar{\eta}^N(0)^\top \ \dot{\bar{\eta}}^N(0)^\top \ \bar{\tau}_{b0}^N(0)^\top]^\top| \leq \sigma/2$ for $t \in [0 \ T_2]$.

Lemma 3. *For $t_f \triangleq min\{T_1, T_2\}$, there exists ϵ_η^* such that the solutions of (24) initiated from any $\xi(0)$ and $\zeta(0)$ satisfies*

$$|[\tilde{\xi}^\eta(t)^\top \ \tilde{\zeta}^\eta(t)^\top]^\top| \leq \lambda_1 e^{-\lambda_2 (t/\epsilon_\eta)} |[\tilde{\xi}^\eta(0)^\top \ \tilde{\zeta}^\eta(0)^\top]^\top| + \Omega(\epsilon_\eta) \quad (25)$$

for $\forall \ t \in [0 \ t_f]$ and $0 < \epsilon_\eta \leq \epsilon_\eta^*$, with some positive constants λ_1 and λ_2, and a class-$\mathcal{K}$ function Ω.

Proof: The proof of Lemma 3 is presented in [17]. ■

From the quasi-steady state results in (19) and (21), the reduced model of (8) is derived as

$$\begin{aligned} \ddot{\eta} &= F_\eta + G_\eta(\tau_{b0} + (\Lambda_\eta \bar{G}_\eta)^{-1} \Pi(u^{\eta *})) + \Delta_\eta \\ &= F_\eta + G_\eta \tau_{b0} + G_\eta \bar{G}_\eta^{-1} u^{\eta *} + \Delta_\eta \\ &= \bar{F}_\eta + \bar{G}_\eta \tau_{b0} \end{aligned} \quad (26)$$

which is exactly identical to the nominal model of WP mode (9). From Remark 4 and Lemma 3, $|[\eta(0)^\top \ \dot{\eta}(0)^\top \ \tau_{b0}(0)^\top]^\top - [\bar{\eta}^N(0)^\top \ \dot{\bar{\eta}}^N(0)^\top \ \bar{\tau}_{b0}^N(0)^\top]^\top| \leq \sigma/2$ for $t \in [0 \ T_2]$ holds and $|[\tilde{\xi}^\eta(t_f)^\top \ \tilde{\zeta}^\eta(t_f)^\top]| \to 0$ as $\epsilon_\eta \to 0$. From those aspects, we can show the result of Theorem 1 by applying Tikhonov's theorem for the infinite time interval presented in [20, p.456].

2) ST and FF modes: Due to Theorem 1 in [17] and [18], for a given $\sigma > 0$, the inequality $|[\chi(t)^\top \ \dot{\chi}(t)^\top \ u_0(t)^\top]^\top - [\bar{\chi}^N(t)^\top \ \dot{\bar{\chi}}^N(t)^\top \ u_0^N(t)^\top]^\top| \leq \sigma$ holds in $\forall t > 0$ if the condition $[\chi(0)^\top \ \dot{\chi}(0)^\top \ u_0(0)^\top]^\top = [\bar{\chi}^N(0)^\top \ \dot{\bar{\chi}}^N(0)^\top \ u_0^N(0)^\top]$ is satisfied.

D. Stability and Robustness Analysis for the Entire Operation

It is shown that the union of $\bar{v}_{WP}^N$, $\bar{v}_{ST}^N$ and $\bar{v}_{FF}^N$ is a σ-robust $WP \mapsto ST$ and $ST \mapsto FF$ transition maneuver. Also, with the condition $\sigma \leq \delta_\eta$, η in ST mode unconditionally reaches $\mathcal{G}\{(ST, FF)\}$ in a finite time since $\|[\eta^\top \tau_b^\top]^\top - [\bar{\eta}^N \tau_{b,0}^\top]^\top\| \leq \|v_{ST} - \bar{v}_{ST}^N\| \leq \sigma \leq \delta_\eta$ is proved to be valid in ST mode. Subsequently, it is also proved that the actual value of x_r and x_q throughout the whole three modes satisfies the inequalities $\|[x_r^\top u_f^\top]^\top - \bar{v}_{WP}^N\| \leq \sigma$ and $\|[x_q^\top u_f^\top]^\top - \bar{v}_{ST \text{ or } FF}^N\| \leq \sigma$ when the initial values of the solutions from the nominal and actual models are identical. Therefore, the stability and robustness of the whole plug-pulling task with the trajectories (4)-(6) and the proposed control structure are guaranteed.

(a) Overall view (b) Detail view

Fig. 5: The stand for a 110 V socket used for the plug-pulling experiment

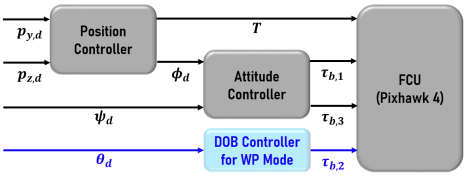

Fig. 6: Strategy for generating control input u in WP mode while conducting the actual experiment. We use the controller presented in [17] for the position and attitude control.

VI. EXPERIMENTAL RESULT & DISCUSSION

A. Experimental Setup

The experimental setup for this study consists of three parts: a hexacopter, a robotic arm, and a frame for the plug-socket system. We assembled the hexacopter with the off-the-shelf frame DJI F550, six KDE2315XF-967 motors with corresponding KDEXF-UAS35 35A+ electronic speed controllers and 9-inches T-Motor polymer rotors, two Turnigy LiPo batteries for power supplement, and Intel NUC for computing. It executes the proposed DOB controller, the Kalman filter for estimating the value of $\ddot{\gamma}$ and the navigation algorithm with OptiTrack on Robot Operating System (ROS) in Ubuntu 18.04, and a flight controller Pixhawk 4, all on-board. The robotic arm is comprised of ROBOTIS dynamixel XH430 and XM540 servo motors. We manufacture a stand for a 110 V socket and firmly attach it to the wooden plate which weighs about 11 kg as in Fig. 5.

As depicted in Fig. 1, the plug is connected to a wire held by the end-effector. Since this is different from the perching model described in Fig. 2, we modify some strategies for the trajectory generation and the controller design to maintain the end-effector's position fixed. For this, we turn on the position controller in $\hat{j}_I$ and $\hat{k}_I$ directions as in Fig. 6.

We set θ_m as 20 deg and the stabilizing time $t_{d,ST} - t_{0,ST}$ as 0.08 sec. Also, the threshold for the mode change from ST to FF, δ_η, is set as 5 deg.

The scenario of the experiment is as follows. At first, the aerial manipulator takes off until the end-effector aligns with the plug attached to the socket. Then, the vehicle flies in $-\hat{i}_I$ direction to tighten the wire. When the wire becomes tight enough, we send a command to begin the WP mode and the vehicle gradually tilts its body. By the time when the plug is separated from the socket, we manually switch to ST mode and the vehicle automatically turns into FF mode when the Euler angles become reasonably small. Finally, the aerial manipulator returns to the original position and maintains the hovering state.

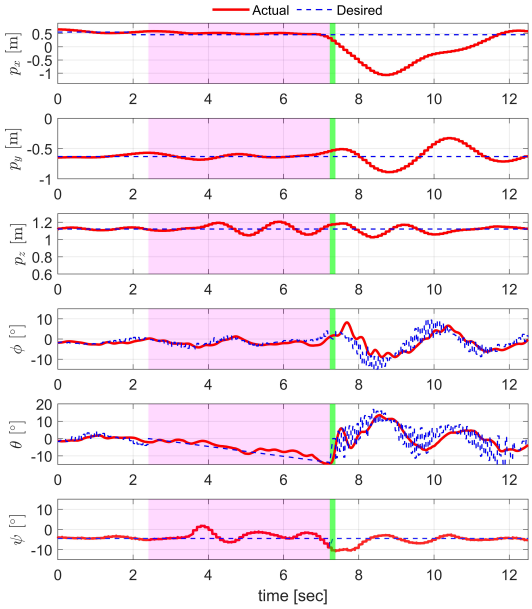

Fig. 7: History of the states of multirotor through the entire operative modes. A white region expresses the FF mode, a magenta region expresses the WP mode and a green region expresses the ST mode. The dashed blue line describes the desired values of the states. The red line represents the measured values of the states.

B. Experimental Results

Fig. 7 shows that the measured value of θ adequately follows θ_d until it reaches -14.4 deg. From this result, we can confirm that the control structure introduced in (9) is valid for the given task. Also, from the plots of p_x, p_y and p_z in Fig. 7, we can observe that the aerial manipulator recovers its original position at about 12 sec. This result shows that the hybrid automata of the aerial manipulator conducting the plug-pulling are stable and robust to the sudden change of interaction force.

On the other hand, as can be seen in the attached video, if a standard PID controller is employed for the wire-pulling, θ cannot adequately follow the desired value θ_d. Accordingly, after the plug is separated from the socket, the vehicle fails to maintain its stability and crashes to the floor.

VII. CONCLUSION

This paper presents an aerial manipulator consisting of a multirotor and a 2-DOF robotic arm pulling a plug out of a socket. To demonstrate aerial plug-pulling, the concept of hybrid automata is used to divide the mission into three operative modes of wire-pulling, stabilizing, and free-flight. The strategy for trajectory generation and design of DOB controllers based on the dynamical models of each operative mode are presented. Then, we prove the overall stability and robustness of the plug-pulling and validate them through the actual experiment. As a result, we confirm that the pitch angle can robustly track the desired pitch trajectory by our proposed DOB controller, and the overall sequence of the plug-pulling task is executed without destabilization. For future work, autonomous grasping of a plug with an aerial manipulator can be included.

REFERENCES

[1] S. Kim, S. Choi, and H. J. Kim, "Aerial manipulation using a quadrotor with a two dof robotic arm," in *2013 IEEE/RSJ International Conference on Intelligent Robots and Systems*. IEEE, 2013, pp. 4990–4995.

[2] H. Kim, H. Seo, J. Kim, and H. J. Kim, "Sampling-based motion planning for aerial pick-and-place," in *2019 IEEE/RSJ International Conference on Intelligent Robots and Systems (IROS)*. IEEE, 2019, pp. 7402–7408.

[3] C. Korpela, M. Orsag, and P. Oh, "Towards valve turning using a dual-arm aerial manipulator," in *2014 IEEE/RSJ International Conference on Intelligent Robots and Systems*. IEEE, 2014, pp. 3411–3416.

[4] S. Kim, H. Seo, and H. J. Kim, "Operating an unknown drawer using an aerial manipulator," in *2015 IEEE International Conference on Robotics and Automation (ICRA)*. IEEE, 2015, pp. 5503–5508.

[5] A. Jimenez-Cano, J. Braga, G. Heredia, and A. Ollero, "Aerial manipulator for structure inspection by contact from the underside," in *2015 IEEE/RSJ international conference on intelligent robots and systems (IROS)*. IEEE, 2015, pp. 1879–1884.

[6] H. Lee and H. J. Kim, "Estimation, control, and planning for autonomous aerial transportation," *IEEE Transactions on Industrial Electronics*, vol. 64, no. 4, pp. 3369–3379, 2016.

[7] J. Byun, D. Lee, H. J. Kim, and H. Lee, "On-line parameter estimation of a hexacopter equipped with 2-dof robotic arm against disturbance," in *2020 20th International Conference on Control, Automation and Systems (ICCAS)*. IEEE, 2020, pp. 47–52.

[8] D. Lee, H. Seo, D. Kim, and H. J. Kim, "Aerial manipulation using model predictive control for opening a hinged door," in *2020 IEEE International Conference on Robotics and Automation (ICRA)*. IEEE, 2020, pp. 1237–1242.

[9] R. Goebel, R. G. Sanfelice, and A. R. Teel, "Hybrid dynamical systems," *IEEE control systems magazine*, vol. 29, no. 2, pp. 28–93, 2009.

[10] J. Back and H. Shim, "An inner-loop controller guaranteeing robust transient performance for uncertain mimo nonlinear systems," *IEEE Transactions on Automatic Control*, vol. 54, no. 7, pp. 1601–1607, 2009.

[11] L. Marconi, R. Naldi, and L. Gentili, "A control framework for robust practical tracking of hybrid automata," in *Proceedings of the 48h IEEE Conference on Decision and Control (CDC) held jointly with 2009 28th Chinese Control Conference*. IEEE, 2009, pp. 661–666.

[12] J. L. Scholten, M. Fumagalli, S. Stramigioli, and R. Carloni, "Interaction control of an uav endowed with a manipulator," in *2013 IEEE International Conference on Robotics and Automation*. IEEE, 2013, pp. 4910–4915.

[13] G. Darivianakis, K. Alexis, M. Burri, and R. Siegwart, "Hybrid predictive control for aerial robotic physical interaction towards inspection operations," in *2014 IEEE international conference on robotics and automation (ICRA)*. IEEE, 2014, pp. 53–58.

[14] A. Praveen, X. Ma, H. Manoj, V. L. Venkatesh, M. Rastgaar, and R. M. Voyles, "Inspection-on-the-fly using hybrid physical interaction control for aerial manipulators," in *2020 IEEE/RSJ International Conference on Intelligent Robots and Systems (IROS)*. IEEE, 2020, pp. 1583–1588.

[15] L. Marconi and R. Naldi, "Control of aerial robots: Hybrid force and position feedback for a ducted fan," *IEEE Control Systems Magazine*, vol. 32, no. 4, pp. 43–65, 2012.

[16] D. Cabecinhas, R. Naldi, C. Silvestre, R. Cunha, and L. Marconi, "Robust landing and sliding maneuver hybrid controller for a quadrotor vehicle," *IEEE Transactions on Control Systems Technology*, vol. 24, no. 2, pp. 400–412, 2016.

[17] D. Lee, H. Seo, I. Jang, S. J. Lee, and H. J. Kim, "Aerial manipulator pushing a movable structure using a dob-based robust controller," *IEEE Robotics and Automation Letters*, 2020.

[18] S. Kim., S. Choi, H. Kim, J. Shin, H. Shim, and H. J. Kim, "Robust control of an equipment-added multirotor using disturbance observer," *IEEE Transactions on Control Systems Technology*, vol. 26, no. 4, pp. 1524–1531, 2017.

[19] J. S. Bang, H. Shim, S. K. Park, and J. H. Seo, "Robust tracking and vibration suppression for a two-inertia system by combining backstepping approach with disturbance observer," *IEEE transactions on industrial electronics*, vol. 57, no. 9, pp. 3197–3206, 2009.

[20] H. K. Khalil and J. W. Grizzle, *Nonlinear systems*. Prentice hall Upper Saddle River, NJ, 2002, vol. 3.